Enhancing the rheological properties and thermal stability of 1 oil-based drilling fluids by synergetic use of organo-montmorillonite and organo-sepiolite

Guanzheng Zhuang, Zepeng Zhang, Shanmao Peng, Jiahua Gao, Maguy Jaber

▶ **To cite this version:**

HAL Id: hal-01957994

https://hal.sorbonne-universite.fr/hal-01957994

Submitted on 17 Dec 2018

Enhancing the rheological properties and thermal stability of oil-based drilling fluids by synergetic use of organo-montmorillonite and organo-sepiolite

Guanzheng Zhuang [a], Zepeng Zhang [a,*], Shanmao Peng [a], Jiahua Gao [a], Maguy Jaber [b,*]

[a] Beijing Key Laboratory of Materials Utilization of Nonmetallic Minerals and Solid Wastes, National Laboratory of Mineral Materials, School of Materials Science and Technology, China University of Geosciences, Xueyuan Road, Haidian District, Beijing 100083, PR China.

[b] Sorbonne Université, Laboratoire d'Archéologie Moléculaire et Structurale (LAMS), CNRS UMR 8220, case courrier 225, UPMC 4 Pl. Jussieu, 75005 PARIS CEDEX 05, France.

Corresponding Author:

Zepeng Zhang

Tel: +86-010-8232-1845

Email: unite508@163.com

Maguy Jaber

Tel: +33-(0)1-4427-6289

Email: maguy.jaber@upmc.fr

Abstract

This work focused on improving the rheological properties and thermal stability of oil-based drilling fluids by using the mixture of organo-montmorillonite (OMt) and organo-sepiolite (OSep) as the rheological additive. OMt and OSep were prepared in water. X-ray diffraction (XRD), scanning electron microscope and transmission electron microscope were applied to characterize the structure of organoclays (OC). The OC/oil gels were characterized using an appropriate XRD method. Dynamic rheological test was used to appraise the rheological behavior, viscosity, gel strength and thixotropy of OC/oil fluids aged at different temperatures. OMt firstly swelled in oil at low temperature, and then exfoliated above 150°C. OSep maintained its crystal structure all the time. The mixing of these two OC did not obviously influence their structures. However, the gel formation ability was promoted, resulting in improvement of rheological properties and thermal stability of oil-based drilling fluids. The nanolayers of OMt and nanofibers of OSep interweaved with each other, reinforcing the network structure and protected them form collapse at high temperatures. The mixture of OMt and OSep with mass proportion of 50% for each displayed the optimal rheological properties and thermal ability.

1. Introduction

Over the next 30 years, global energy is projected to rise almost 60%, a challenging trend that may be met only by revolutionary breakthroughs in energy science and technology (Esmaeili, 2011). Although the technologies of some new or renewable energies (such as new battery, wind energy, nuclear energy, etc.) are developing fast, oil and gas, as the traditional energy, are the main energy resource in the world. The demand of oil and gas is increasing due to the rapid development of the society. However, the petroleum industry is increasingly drilling more technically challenging and difficult wells. Drilling of deeper wells worldwide requires constants searching for adequate drilling fluids to overcome extreme conditions (Williams et al., 2011).

Drilling fluids are compared as "the bloods of drilling operations". By drilling operations, oil and gas can be extracted from the earth. Drilling fluids serve several fundamental functions, such as (i) to remove the cuttings generated by the drill bit from the borehole, (ii) to control the downhole formation pressures, (iii) to overcome the fluid pressure of the formation, (iv) to avoid damage to the producing formation and (v) to cool and lubricate the drill bit, etc. (Chilingarian and Vorabutr, 1983; Caenn and Chillingar, 1996; Meng et al., 2012). Generally, drilling fluids can be divided into two types based on the continuous phase, i.e., water-based drilling fluids and oil-based drilling fluids. Water-based drilling fluids are limited by their abilities of dissolving salts, interfering with the flow of oil and gas through porous rocks, promoting the disintegration and dispersion of clay minerals, and effecting the corrosion of iron

67 (Caenn et al., 2011). Oil-based drilling fluids, owing to their excellent lubricity, high

68 rate of penetration, shale inhibition, wellbore stability, high lubricity, high thermal

69 stability (Caenn and Chillingar, 1996; Khodja et al., 2010), are advised to be used to

70 drill difficult wells. In spite of the advantages of oil-based drilling fluids, drilling

71 practice always demand drilling fluids with greater rheological properties and better

72 thermal stability.

73   Organoclays (OC) are used in oil-based drilling fluids to control the rheological

74 behavior. They perform specific functions in a base oil and are varied in amount to

75 furnish the properties required for satisfying the conditions of use. Organo-

76 montmorillonite (OMt) is mostly used in oil-based drilling fluids (Caenn et al., 2011;

77 Dino and Thompson, 2013; Zhuang et al., 2016, 2017b). Hermoso et al. (2014) reported

78 that the viscous flow behavior of oil-based drilling fluids is deeply influenced by OMt

79 nature and concentration. (Schmidt, 1987) proposed that OC did not viscosify the oils

80 but built the structure through interactions with the aqueous face (water phase is usually

81 included in oil-based drilling fluids). But later work (Burgentzle et al., 2004)

82 demonstrated that OMt can viscosify organic solvents without water. Previous work

83 (Zhuang et al., 2017b, d) reported the exfoliation of OMt in oil aged at high

84 temperatures. Exfoliated OMt produced many nanolayers to build a "house of cards"

85 structure, resulting in the improvement of gel formation and rheological properties. By

86 comparing studies on different modifiers, surfactants containing two long alkyl chains

87 was proved to be easier to result in exfoliation of OMt in oil and excellent rheological

88 properties. However, distinct decline of the rheological properties occurred when best

89   fluids aged above 180°C, because of two potential ways, i.e., thermal decomposition

90   and desorption of organic surfactants.

91   Recently, the OC from palygorskite-sepiolite family were reported to be used in oil-

92   based drilling fluids (Dino and Thompson, 2002; Zhuang et al., 2017a, c, d, 2018b;

93   Weng et al., 2018). They exhibited excellent rheological properties in oil by forming a

94   "haystack" structure. These clay minerals are natural nanofibrous materials. For

95   sepiolite (Sep), its fiber sizes generally range from 0.2 μm to 2 μm in length, 100 nm to

96   300 nm in width and 50 nm to 100 nm in thickness (Alvarez, 1984; Álvarez et al., 2011).

97   Accordingly, Sep shows preeminent rheological properties in polar solvents. By organic

98   modification, organo-sepiolite (OSep) displays the lipophilicity and can perform

99   excellent rheological properties in oil (Zhuang et al., 2018a).

100   Some recent literature reported about the joint use of Mt and fibrous clay minerals

101   (Neaman and Singer, 2000; Chemeda et al., 2014; Al-Malki et al., 2016) to enhance the

102   rheological properties of clay minerals in solvents. Al-Malki et al. (2016) found that

103   bentonite-based drilling mud with Sep nanoparticles showed a great stability in plastic

104   viscosity and yield point over a wide range of temperature and pressure, especially at

105   high temperatures and pressures. The previous work enlightened that synergistic use of

106   OMt and OSep may also promote the rheological properties and thermal stability of oil-

107   based drilling fluids. This is a promising way to sustain oil-based drilling fluids work

108   in difficult wells.

109   Aiming to improve the rheological properties and thermal stability of oil-based

110   drilling fluids, OMt and OSep was synergistically used in oil-based fluids aged at

5

111 different temperatures and their structures and rheological properties were

112 characterized.

113

114 2. Materials and Methods

115 2.1 Materials

116   Na$^+$-treated Mt was obtained from Kazuo, Liaoning, China, with the purity of ca.

117 84% and cation exchange capacity (CEC) of 120 cmol/kg. Sep was obtained from Spain,

118 with the CEC of 35 cmol/kg. The purity of clay minerals was defined X-Ray diffraction

119 method according to the Chinese standard SY/T 5163-2010. Details of this method were

120 reported in previous literature (Zhuang et al., 2018a). Some quartz (12%), calcite (4%)

121 and albite (2%) were included in the Mt sample (see Fig. 1 (A)). XRD pattern of Sep

122 (Fig. 1 (B)) matches well with the JCPDS card of Sep and no other reflections are

123 observed, indicating the high purity of Sep. The chemical composition of Mt and Sep

124 were characterized by X-ray fluorescence (XRF) analysis and the results are listed in

125 Table 1. Both of these two clay minerals were milled and sieved with a 200-mesh sieve

126 before use. Benzyl dimethyl octadecyl ammonium chloride (C18, purity of 97%) and

127 dimethyl dioctadecyl ammonium chloride (DC18, purity of 98%) were bought from

128 Anhui Super Chemical Technology Co., Ltd, China. The white oil (No. 5) was bought

129 from China National Petroleum Corporation.

130

131 2.2 Preparation of OC

132   OMt was prepared in aqueous solution as the following steps: 100 g of Mt was

133   added into 1 L deionized water, stirring for 0.5 h; then DC18 (1.0 CEC of Mt) was

134   added into the previous dispersion, stirring for 1 h; at last, by centrifugation, drying at

135   60°C for 24 h, milling and sieving with a 200-mesh sieve. OSep was prepared as the

136   following steps: C18 (35% of the mass of Sep) was firstly dissolved into 500 mL

137   distilled water (keep at 60°C in the whole process), 100 g of Sep was added into the

138   previous solution, stirred for 1 h and thickened slurry was obtained; at last, after drying

139   at 60°C for 24 h, milling and sieving with a 200-mesh sieve, OSep was prepared.

140   2.3 Preparation of Sep/oil fluids

141   12 g of OC was added into 400 mL white oil (concentration of 30 kg/m^3) and

142   blended at 10000 rpm for 20 min. A drilling fluid should be aged at different

143   temperatures to model the real drilling operation. According to the standards of API

144   SPEC 13A and API RP 13B-2, the resulting fluid was placed in a rotary oven heated to

145   66°C, 150°C, 180°C and 200°C where it was aged for 16 h. The mixtures of OC in oil-

146   based drilling fluids are listed in Table 2. The corresponding fluid is named as OC/oil-

147   temperature. For example, the oil-based fluid of OMt$_{0.5}$-OSep$_{0.5}$ and oil aged at 150°C

148   is named as OMt$_{0.5}$-OSep$_{0.5}$/oil-150.

149

150   2.4 Characterization

151   The X-ray diffraction (XRD) analysis was conducted on a Bruker D8 Advance X-

152   ray powder diffractometer operating at Cu Kα radiation, 40 kV, 40 mA and a scan speed

153   of 0.05 s per step (step size: 0.02°). The XRD patterns were collected from 3° to 70°.

154   Particularly, the XRD test for OC/oil gels is described in the section 3.1. Scanning

155   electron microscope (SEM) images were obtained with a HITACHI SU8000 type SEM

156   and the operating voltage was 10 kV. The transmission electron microscope (TEM)

157   analysis was conducted on a JEM 1200EX TEM equipment and operated at the voltage

158   of 200 kV. Gel volume results were obtained by adding 100 mL aged fluid into a

159   graduated cylinder with a stopper and standing for 24 h. The dynamic rheological

160   behavior of oil-based fluids was tested by a Thermo Scientific HAAKE Roto Visco 1

161   rotational viscometer at 20°C. The tested program was: the shear rate linearly increased

162   from 0 s^{-1} to 100 s^{-1} in 5 min (up step), and then linearly decreased from 100 s^{-1} to 0 s^{-}

163   ^{1} in 5 min (down step).

164

165   3. Results and discussion

166   3.1 XRD analysis

167   The XRD patterns of Mt and OMt were presented in Fig. 1 (A). There were some

168   impurities, i.e., quartz and calcite in the Mt sample. The basal reflection of Mt occurred

169   at $2\theta = 7.05°$, with the basal spacing of 1.25 nm. Modified with DC18, a group of

170   reflections emerged at 2.40°, 4.82° and 7.34°, which were attributed to the reflections

171   of (001), (002) and (003) crystalline planes. The basal spacing of OMt increased to 3.68

172   nm, indicating the successful intercalation of DC18 into the interlayer space. In Fig. 1

173   (B), the XRD pattern of OSep is nearly the same with that of Sep. This phenomenon

174   demonstrated that the organic modification could not influence the crystal structure of

175   Sep, similar with the modification of palygorskite (Zhuang et al., 2017a, c). This is

176   because that the TOT (T refers [SiO_4] tetrahedron and O refers to [$Al(Mg)O_6$]

8

177　octahedron) layers were linked by covalent bonds. Based on the TGA results (see Fig.

178　S1, in supplementary materials), there were 40.8% and 23.4% of organic surfactants

179　included in OMt and OSep, respectively.

180　　The OC/oil gels were also characterized by XRD using an appropriate method (see

181　Fig. 2 (A)). Firstly, the OC/oil fluid was dripped on oil-absorbing papers. After 24 h of

182　natural absorption, extra oil was removed and the OC/oil gel was obtained. OC/oil gels

183　were marked following the template of "OC/oil-temperature". Finally, the OC/oil gels

184　can be tested using the X-ray diffractometer similar with powder samples. The XRD

185　patterns of sample holder and sample holder with oil are shown in Fig. 2 (B). The

186　sample holder exhibited a small reflection with low intensity. However, a wider

187　reflection occurred in the XRD pattern of sample holder + oil, with higher intensity.

188　These two reflections are typical amorphous ones, in agreement with the previous

189　literature (Ribotta et al., 2004; Bates et al., 2006; Ford et al., 2010; Rowe and Brewer,

190　2017). Thus, this reflection between 8 to 30° and centering at ca. 17° is assigned to the

191　amorphous reflection of oil.

192　　The XRD patterns of OC/oil gels aged at different temperatures are presented in Fig.

193　3. A wide reflection in the range of $2\theta = 8\text{-}30°$ emerged in the XRD patterns of OC/oil

194　gels, centering at 17 to 18°. They are attributed to the oil as proved in Fig. 2 (B). These

195　wide reflections demonstrated that oil molecules were packaged in the network

196　structures of OC. The intensity of these reflections can be used to evaluate the oil

197　contents in the gels. Compared with OMt, the XRD patterns of OMt/oil-66 and $OMt_{0.8}$-

198　$OSep_{0.2}$/oil-66 showed that the basal spacing of OMt in these two gels increased to 5.04

nm: indeed, oil molecules are probably in the interlayer space due to the lipophilicity.

In the XRD pattern of $OMt_{0.5}$-$OSep_{0.5}$/oil-66, both intensities of reflections attributed to OMt and OSep dramatically reduced, indicating disordered arrangements parallel to the c-axis of OMt and the b-axis of OSep. When the mass content of OSep increased to 80%, the basal reflection of OMt disappeared in the XRD pattern of $OMt_{0.2}$-$OSep_{0.8}$/oil-66. Considering the changes in the XRD patterns of $OMt_{0.5}$-$OSep_{0.5}$/oil-66 and $OMt_{0.2}$-$OSep_{0.8}$/oil-66, the mixing of OMt and OSep facilitated the exfoliation of OMt. The XRD pattern of OSep/oil-66 is similar with that of OSep powder, in spite of the wide reflection from 8° to 30°.

With the temperature rising, the wide reflection of oil showed high intensity, indicating more oil molecules contained in the gel structures. This fact proved that high temperatures promoted the formation of a stronger network structure with large interspace. OSep/oil gels maintained the reflections of Sep at different temperatures. However, the basal reflections of OMt/oil gels aged above 150°C disappeared, probably suggesting the exfoliation of OMt. But the (100) reflection, which emerged at $2\theta =$ 19.7°, was kept in the XRD patterns of OMt/oil gels. This phenomenon implied that the individual TOT structures were kept and changes just happened to the arrangement paralleling to the c-axis. The basal reflection of OMt was not observed in the mixture of OMt and OSep aged at high temperatures, indicating the exfoliation of OMt. With the increase of OSep, OC/oil gels exhibited higher intensity of the (110) reflection, because of the more proportion of OSep. Significantly, the XRD patterns of these OC/oil aged from 150°C to 200°C showed the similar reflections, indicating that they

221   kept the structures in this temperature range.

223   3.2 SEM and TEM

224   The SEM and TEM images are presented in Fig. 4. OMt is associated with a large

225   number of silicate layers. To some extent, these layers are soft so that they may be

226   curved. Based on the TEM image of OMt, the lamellae contain at least 10 layers. The

227   distance between two adjacent layers was measured as 3.56 nm. This value is a little

228   smaller than the basal spacing derived from the XRD result. This is because the high

229   voltage of TEM test (200 kV) would destroy the interlayer surfactants and/or

230   dehydration of the interlayer space (Kogure, 2013). Hence, the basal spacing calculated

231   from the TEM depended on the voltage, test time, thermal stability of organic

232   compounds and the thickness of samples. The exfoliation of OMt was defined as no

233   further interaction occurs between the two delaminated units (isolated layers or stacking

234   of few layers) which become independently mobile in the liquid phase (Bergaya et al.,

235   2012), so that the no long-range order was apparent along the c-axis. The exfoliated

236   OMt layers would form a "house of cards" structure by surface to edge and edge to

237   edge arrangements.

238   The SEM and TEM images of OSep showed the disordered aggregation of OSep

239   fibers. The length of fibers ranged from hundreds of nanometers to ca. 1 μm. Indeed,

240   the OSep existed in the forms of individual fibers (rods), laths and bundles (García-

241   Romero and Suárez, 2013). The crystal laths and bundles, which consist of nanofibers,

242   are very hard to be disaggregated, due to the electronic attraction, Van der Waals forces

243 and hydrogen bonding interaction (Haden and Schwint, 1967; Xu et al., 2014). The

244 aggregation of different forms of OSep built a "haystack" structure (Haden, 1963).

245   The SEM or TEM images of OC/oil gels can't be obtained, because of the high

246 amount of oil present in the gels. Indeed, it is difficult to remove the oil because of its

247 high boiling point and non-volatile ability.

248

249 3.3 Gel volume

250   The gel volume results (see Fig. 5) can directly show the gel formation ability and

251 compatibility between oil and OC. At the initial time (t = 0 s), all the gel volumes of

252 OC/oil fluids were set as 100.0 mL. When the time went to 90 min, the gel volumes of

253 OMt, $OMt_{0.8}$-$OSep_{0.2}$, $OMt_{0.5}$-$OSep_{0.5}$, $OMt_{0.2}$-$OSep_{0.8}$ and OSep in oil were 21.8 mL,

254 97.2 mL, 98.0 mL, 100.0 mL and 100.0 mL, respectively. After standing four 24 h, the

255 gel volumes became 15.7 mL for OMt, 67.1 mL for $OMt_{0.8}$-$OSep_{0.2}$, 89.5 mL for

256 $OMt_{0.5}$-$OSep_{0.5}$, 100.0 mL for $OMt_{0.2}$-$OSep_{0.8}$ and 100.0 mL for OSep. OMt showed

257 the least gel volume in oil while OSep presented the gel volume of 100.0 mL. At room

258 temperature, OMt can only absorb a part of oil molecules, resulting in the expanding of

259 interlayer space. The swelling OMt particles dispersed and stacked in oil, without

260 prominent contributions to promoting the network structure and gel formation.

261 However, TEM images testified that OSep is in the form of fibers, laths and bundles,

262 which are in nanoscale. These fibers laths and bundles could be easier to form "haystack"

263 structures, leading to the high and stable gel volumes. The gel volumes of OMt/OSep

264 mixture in oil increased with the increase of OSep proportion. This phenomenon

265 suggested that the addition of OSep contributed to the gel formation of OMt in oil.

266

267 3.4 Rheological properties

268 The dynamic rheological curves of OC/oil fluids are presented in Fig. 6. These

269 curves display the rheological behavior and thermal stability of corresponding OC/oil

270 fluids. Aged at 66°C, OMt/oil fluid showed the highest shear stress, indicating that

271 OMt/oil fluid displayed the best viscosity. OMt/oil and OSep/oil fluids aged at 66°C

272 showed the different curves of up step and down step. However, in the rheological

273 curves of the mixture of OMt and OSep fluids, the down step curves nearly followed

274 the up step curves. This fact demonstrated that the network structures of OMt and

275 OSep in oil obviously changed while no distinct structural changes happened in the

276 mixture fluids. The single OC built their own network structures in oil. But the new

277 network structure didn't form well in the mixed oil fluids aged at 66°C. In addition,

278 the rheological curves of fluids aged at 66°C followed the Bingham plastic model at

279 10-100 s^{-1}, except for OSep/oil aged at 66°C.

280 When the temperature increased to above 150°C, the rheological curves became

281 very different. Firstly, the shear stresses of fluids aged above 150°C is much larger

282 than those of fluids aged at 66°C, demonstrating the promotion of network structures

283 and viscosity by high temperatures. Furthermore, in the up step, a rapid climb was

284 observed before 20 s^{-1}, and then a dramatical decline occurred. Consequently, there

285 was a critical point which showed the highest shear stress. This critical point

286 suggested that a large shear stress must be applied to break the connected aggregates

13

287   of OC and to disperse and orient stacked nanoplatelets or nanofibers (maybe nano

288   laths and bundles) in the flow direction (Zhuang et al., 2017b). In the down step, the

289   curves were nearly lines (in spite of the derivation at 0-20 s^{-1}), in agreement with the

290   Bingham plastic model. No critical points were seen in the down step because the

291   network had been sheared at high shear rate and the network structures were

292   destroyed.

293   These critical points can indicate the gel strengths of network structures. The

294   shear stress results corresponding to these critical points are listed in Table 3. Aged at

295   66°C, OSep/oil fluid showed a little different rheological curve from other fluids, due

296   to the changes at 0-40 s^{-1} in up step. It was a critical range, instead of a point, because

297   the network structure was not enough strong. The critical shear stresses of OMt/oil

298   and OSep/oil fluids firstly increased and then decreased, indicating that the increase

299   of aging temperature firstly improved the formation of network structure and higher

300   temperature would be harmful for the network structure, due to the thermal

301   degradation and/or desorption of organic surfactants. The critical shear stress of

302    $OMt_{0.8}$-$OSep_{0.2}$/oil fluid gradually decreased with the temperature rising. However,

303    $OMt_{0.5}$-$OSep_{0.5}$/oil and $OMt_{0.2}$-$OSep_{0.8}$/oil fluids showed basically stable critical

304   shear stresses from 150°C to 180°C, and little higher ones at 200°C. This

305   phenomenon demonstrated the better stability of the mixture of OMt and OSep than

306   single OC in oil-based drilling fluids.

307   The shear stresses of samples at 100 s^{-1} were applied to evaluate the viscosities (η)

308   of different fluids (Table 4). As $\eta = \tau/\gamma$ and γ was constant (τ refers to shear stress and

309   γ refers to shear rate), i.e., 100 s^{-1}, τ can be used to indicate the changes of η. Aged at

310   66°C, the τ values of samples were very low, because the OC were not exfoliated

311   completely or dispersed well. With the temperature rising, the τ values dramatically

312   increased due to the fine formation of network structures which was promoted by high

313   temperatures. For example, the τ_{66-150} values of OMt/oil, OMt$_{0.8}$-OSep$_{0.2}$/oil, OMt$_{0.5}$-

314   OSep$_{0.5}$/oil, OMt$_{0.2}$-OSep$_{0.8}$/oil and OSep/oil were 108%, 378%, 687%, 696% and

315   694%. Compared with the τ values at 180°C, OMt/oil, OMt$_{0.8}$-OSep$_{0.2}$/oil and OSep/oil

316   at 200°C decreased by 49%, 26% and 18%. However, the τ values of OMt$_{0.5}$-OSep$_{0.5}$

317   and OMt$_{0.2}$-OSep$_{0.8}$ at 200°C increased by 46% and 18%. These results also supported

318   that the mixture of OMt and OSep benefited the viscosity and thermal stability of oil-

319   base drilling fluids.

320   Thixotropy represents a reversible isothermal transformation of a colloidal sol to

321   a gel. It is caused by the clay mineral units slowly arranging themselves in positions of

322   minimum free energy. In drilling practice, low resistance (low viscosity) is expected for

323   the bit to ensure high drilling rate, while high viscosity is expected for carrying cuttings.

324   Excellent thixotropy of an oil-based drilling fluid is necessary. The areas of thixotropic

325   loops (abbreviated as A, see in Table 5) in Fig. 6 are applied to evaluate the thixotropy

326   of OSep/oil fluids.

327   Aged at 66°C, the A value of OMt/oil fluid was 22.5 Pa·s^{-1} and that of OSep/oil

328   fluid was 39.38 Pa·s^{-1}. The A values of OMt$_{0.8}$-OSep$_{0.2}$/oil, OMt$_{0.5}$-OSep$_{0.5}$/oil and

329   OMt$_{0.2}$-OSep$_{0.8}$/oil fluids ranged from 2.39 to 4.82 Pa·s^{-1}, indicating nearly no

330   thixotropy of these samples. High temperatures promoted the gel formation. The A

331   values of samples increased until aged at 180°C, except for those of $OMt_{0.5}$-$OSep_{0.5}$/oil

332   and $OMt_{0.2}$-$OSep_{0.8}$/oil. The decrease rates of OMt/oil, $OMt_{0.8}$-$OSep_{0.2}$/oil and

333   OSep/oil from 180°C to 200°C ($A_{180-200}$) were 71%, 49% and 24%. OMt/oil declined

334   more than OSep/oil. $OMt_{0.5}$-$OSep_{0.5}$/oil and $OMt_{0.2}$-$OSep_{0.8}$/oil exhibited continuous

335   and slow augment of the A values until to 200°C, so that these two samples can be

336   basically regarded as stable samples. The A values of $OMt_{0.5}$-$OSep_{0.5}$/oil and $OMt_{0.2}$-

337    $OSep_{0.8}$/oil at 150-200°C were much more than those of a single OC, demonstrating

338   that the mixture of OMt and OSep contributed to improving the thixotropy of oil-based

339   fluids.

340   Considering all the discussions of rheological properties, the mixture of OMt and

341   OSep, with the mass proportion of 50% for each, can effectively improve the viscosity,

342   gel strength, thixotropy and thermal stability of the oil-based fluids.

343

344   3.5 Network structure

345   The rheological test proved that the $OMt_{0.5}$-$OSep_{0.5}$ performed greater rheological

346   properties and better thermal stability in oil than each single OC did. This enhancement

347   was resulted by the mixed network structure (see Fig. 7). When mixing OMt and OSep

348   in oil, they firstly disperse following their own nature. At low temperature, oil

349   molecules were adsorbed into the interlayer space of OMt, resulting in swelling. OMt

350   was mostly in the form of swelled particles, perhaps with a little exfoliated nanolayers.

351   OSep fibers, laths and crystal bundles dispersed in oil. Although the mass proportions

352   of these two OC were identical, the number of OMt particles was much less than the

353   number of OSep fibers, laths and bundles. Due to the difference of these numbers, OMt

354   and OSep had no strong contact with each other. But the mixing of these two OC still

355   improved their gel formation in oil (see Fig. 5).

356   As the XRD results demonstrated that OMt exfoliated in oil above 150°C, one OMt

357   particle might divided into dozens or hundreds of nanolayers. Consequently, the number

358   of OMt layers dramatically increased. Influenced by the thermal motion, these

359   nanolayers mixed and contact with the nanofibers, laths and bundles. Significantly, the

360   "house of cards" structure of OMt and the "haystack" structure were not independent.

361   These two different shapes of silicate units (layered OMt and fibrous OSep)

362   interweaved with each other, leading to a stronger network structure. Previous work

363   testified that organic surfactants would decomposed or/and dissolved into oil at high

364   temperature, resulting the shrink of OMt (Zhuang et al. 2017b). In this mixed network

365   structure, exfoliated OMt layers were supported by OSep fibers, and the OSep fibers

366   were also sustained by the nanolayers.

367

368   4. Conclusion

369   In summary, synergetic use of OMt and OSep can improve the rheological

370   properties and thermal stability of oil-based drilling fluids. OMt firstly swelled in oil

371   by adsorbing oil molecules while OSep showed stable dispersion due to its nanoscale

372   fibers, laths and bundles. At high temperature, thermal motion promoted the exfoliation

373   of OMt into nanolayers. The interweave of nanofibers (laths and bundles) of nanolayers

374   enhanced the network structure, resulting in improvement of rheological properties.

375 The mutual support between OMt nanolayers and OSep nanofibers protected this

376 network structure form crush at high temperatures.

377

378 Acknowledgement

383

384 References

385 Al-Malki, N., Pourafshary, P., Al-Hadrami, H., Abdo, J., 2016. Controlling bentonite-

386   based drilling mud properties using sepiolite nanoparticles. Petrol. Explor. Dev.

387   43, 717-723.

388 Alvarez, A., 1984. Sepiolite: properties and uses, in: Tolsa (Ed.), Developments in

389   Sedimentology, pp. 253-287.

390 Álvarez, A., Santarén, J., Esteban-Cubillo, A., Aparicio, P., 2011. Current Industrial

391   Applications of Palygorskite and Sepiolite, in: Singer, A., Galan, E. (Eds.),

392   Developments in Clay Science. Elsevier, Amsterdam, pp. 281-298.

393 Bates, S., Zografi, G., Engers, D., Morris, K., Crowley, K., & Newman, A. (2006).

394   Analysis of amorphous and nanocrystalline solids from their X-ray diffraction

395   patterns. Pharm. res., 23(10), 2333-2349.

396 Bergaya, F., Jaber, M., Lambert, J.F., Chapter 3 Clays and Clay Minerals as Layered

397   Nanofillers for (Bio)Polymers. In: Environmental Silicate Nano-biocomposites,

398   Avérous, L. and Pollet, E (Eds) Springer London. 2012, 41-75

399   Burgentzle, D., Duchet, J., Gerard, J.F., Jupin, A., Fillon, B., 2004. Solvent-based

400   nanocomposite coatings I. Dispersion of organophilic montmorillonite in organic

401   solvents. J. Colloid. Interf. Sci., 278, 26-39.

402   Caenn, R., Chillingar, G.V., 1996. Drilling fluids: State of the art. J. Petrol. Sci. Eng.,

403   14, 221-230.

404   Caenn, R., Darley, H.C., Gray, G.R., 2011. Composition and properties of drilling and

405   completion fluids. Gulf professional publishing, Houston.

406   Chemeda, Y.C., Christidis, G.E., Khan, N.M.T., Koutsopoulou, E., Hatzistamou, V.,

407   Kelessidis, V.C., 2014. Rheological properties of palygorskite-bentonite and

408   sepiolite-bentonite mixed clay suspensions. Appl. Clay Sci., 90, 165-174.

409   Chilingarian, G.V., Vorabutr, P., 1983. Drilling and drilling fluids. Elsevier Scientific

410   Pub. Co. distributors for the U.S. and Canada, Elsevier North-Holland.

411   Dino, D., Thompson, J., 2002. Organophilic clay additives and oil well drilling fluids

412   with less temperature dependent rheological properties containing said additives.

413   US 6462096 B1.

414   Dino, D., Thompson, J., 2013. Organophilic clay additives and oil well drilling fluids

415   with less temperature dependent rheological properties, US8389447 B2.

416   Esmaeili, A., 2011. Applications of Nanotechnology in Oil and Gas Industry, AIP

417   conference proceedings, AIP 1414(1): 133-136.

418   Ford, E. N. J., Mendon, S. K., Thames, S. F., Ph., D., Rawlins, J. W., & Ph., D. (2010).

419   X-ray diffraction of cotton treated with neutralized vegetable oil-based

420   macromolecular crosslinkers. J. Eng. Fiber Fabr., 5(1), 10-20.

421   García-Romero, E., Suárez, M., 2013. Sepiolite–palygorskite: Textural study and

422   genetic considerations. Appl. Clay Sci., 86, 129-144.

423   Haden, W., 1963. Attapulgite: properties and uses. Clays Clay Miner 10, 284-290.

424   Haden, W.L., Schwint, I.A., 1967. Attapulglte: Its properties and applications. Ind. Eng.

425   Chem., 59, 58-69.

426   Hermoso, J., Martinez-Boza, F., Gallegos, C., 2014. Influence of viscosity modifier

427   nature and concentration on the viscous flow behaviour of oil-based drilling fluids

428   at high pressure. Appl. Clay Sci., 87, 14-21.

429   Khodja, M., Canselier, J.P., Bergaya, F., Fourar, K., Khodja, M., Cohaut, N.,

430   Benmounah, A., 2010. Shale problems and water-based drilling fluid optimisation

431   in the Hassi Messaoud Algerian oil field. Appl. Clay Sci., 49, 383-393.

432   Kogure, T., 2013. Chapter 2.9 - Electron Microscopy, in: Bergaya, F., Lagaly, G. (Eds.),

433   Developments in Clay Science. Elsevier, Netherlands, pp. 275-317.

434   Meng, X., Zhang, Y., Zhou, F., Chu, P.K., 2012. Effects of carbon ash on rheological

435   properties of water-based drilling fluids. J. Petrol. Sci. Eng., 100, 1-8.

436   Neaman, A., Singer, A., 2000. Rheology of mixed palygorskite-montmorillonite

437   suspensions. Clay Clay Miner. 48, 713-715.

438   Ribotta, P. D., Cuffini, S., León, A. E., & Añón, M. C. (2004). The staling of bread: an

439   x-ray diffraction study. Eur. Food Res. Technol., 218(3), 219-223.

440   Rowe, M. C., Brewer, B. J. (2017). AMORPH: A statistical program for characterizing

441   amorphous materials by X-ray diffraction. arXiv:1709.04556.

442 Schmidt, D.D., Roos, A. J., & Cline, J. T, 1987. Interaction of water with organophilic

443   clay in base oils to build viscosity. Society of Petroleum Engineers, 311-326.

444 Weng, J., Gong, Z., Liao, L., Lv, G., Tan, J., 2018. Comparison of organo-sepiolite

445   modified by different surfactants and their rheological behavior in oil-based

446   drilling fluids. Appl. Clay Sci., in press, DOI: 10.1016/j.clay.2017.12.031.

447 Williams, R.H., Khatri, D.K., Vaughan, M.L., Landry, G., Janner, L., Mutize, B.,

448   Herrera, M., 2011. Particle size distribution-engineered cementing approach

449   reduces need for polymeric extenders in haynesville shale horizontal reach wells,

450   SPE Annual Technical Conference and Exhibition. Society of Petroleum

451   Engineers.

452 Xu, J., Wang, W., Wang, A., 2014. Dispersion of palygorskite in ethanol–water mixtures

453   via high-pressure homogenization: Microstructure and colloidal properties.

454   Powder Technol., 261, 98-104.

455 Zhuang, G., Zhang, Z., Sun, J., Liao, L., 2016. The structure and rheology of organo-

456   montmorillonite in oil-based system aged under different temperatures. Appl. Clay

457   Sci., 124, 21-30.

458 Zhuang, G., Wu, H., Zhang, H., Zhang, Z., Zhang, X., Liao, L., 2017a. Rheological

459   properties of organo-palygorskite in oil-based drilling fluids aged at different

460   temperatures. Appl. Clay Sci., 137, 50-58.

461 Zhuang, G., Zhang, H., Wu, H., Zhang, Z., Liao, L., 2017b. Influence of the surfactants'

462   nature on the structure and rheology of organo-montmorillonite in oil-based

463   drilling fluids. Appl. Clay Sci., 135, 244-252.

464   Zhuang, G., Zhang, Z., Gao, J., Zhang, X., Liao, L., 2017c. Influences of surfactants on

465   the structures and properties of organo-palygorskite in oil-based drilling fluids.

466   Micropor. Mesopor. Mat., 244, 37-46.

467   Zhuang, G., Zhang, Z., Jaber, M., Gao, J., Peng, S., 2017d. Comparative study on the

468   structures and properties of organo-montmorillonite and organo-palygorskite in

469   oil-based drilling fluids. J. Ind. Eng. Chem., 56, 246-257.

470   Zhuang, G., Gao, J., Chen, H., Zhang, Z., 2018a. A new one-step method for physical

471   purification and organic modification of sepiolite. Appl. Clay Sci., 153, 1-8.

472   Zhuang, G., Zhang, Z., Yang, H., Tan, J., 2018b. Structures and rheological properties

473   of organo-sepiolite in oil-based drilling fluids. Appl. Clay Sci., 154, 43-51.
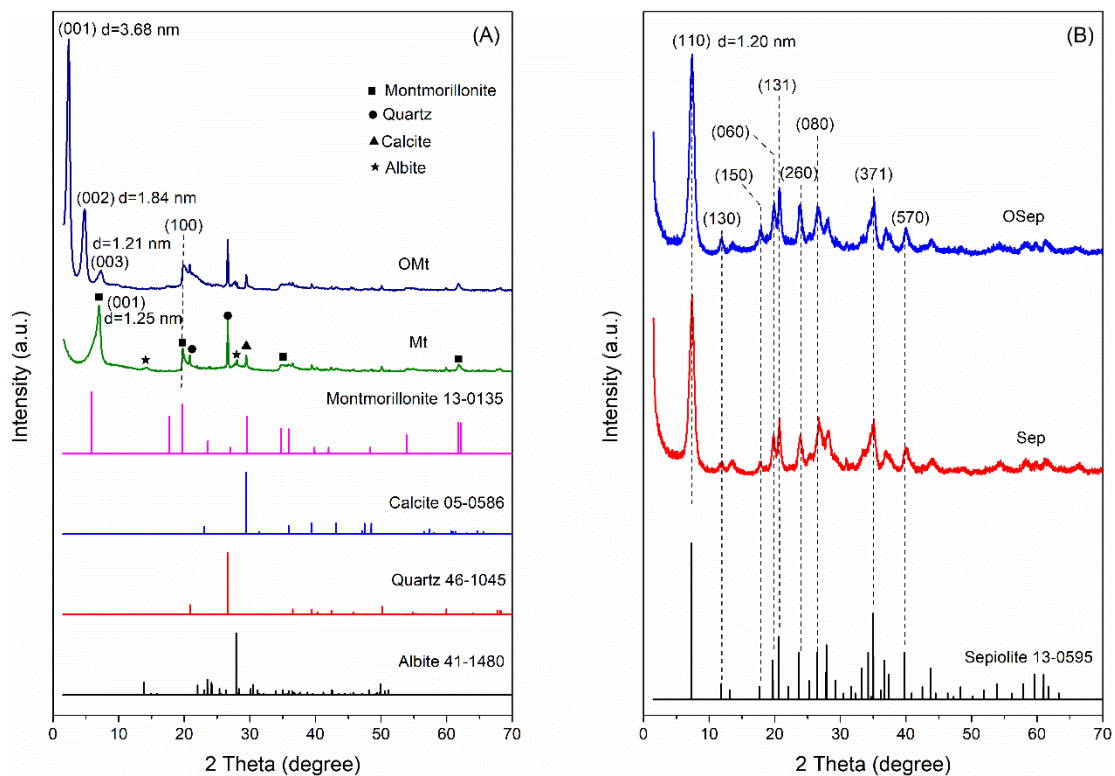
474

475

Figures

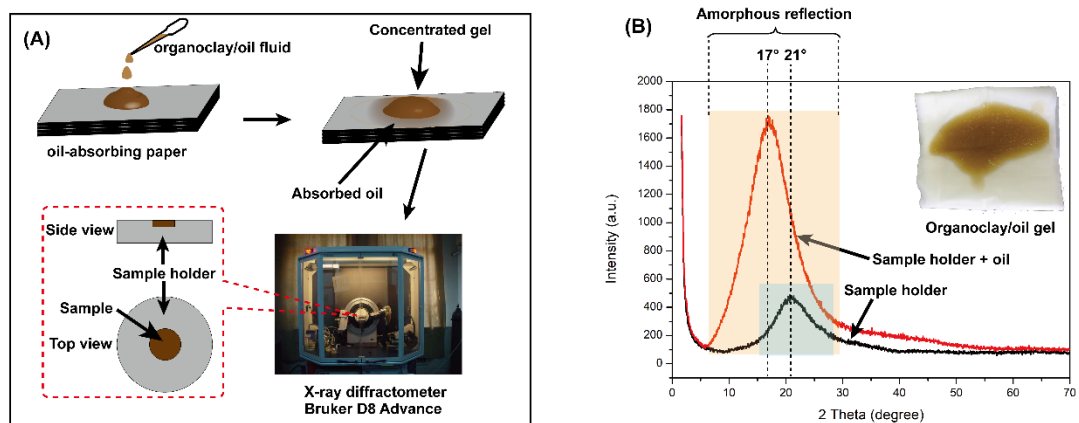Fig. 1 XRD patterns of (A) Mt, OMt, (B) Sep and OSep.

Fig. 2 (A) Interpretive diagram of XRD test for OC/oil gel sample and (B) XRD patterns

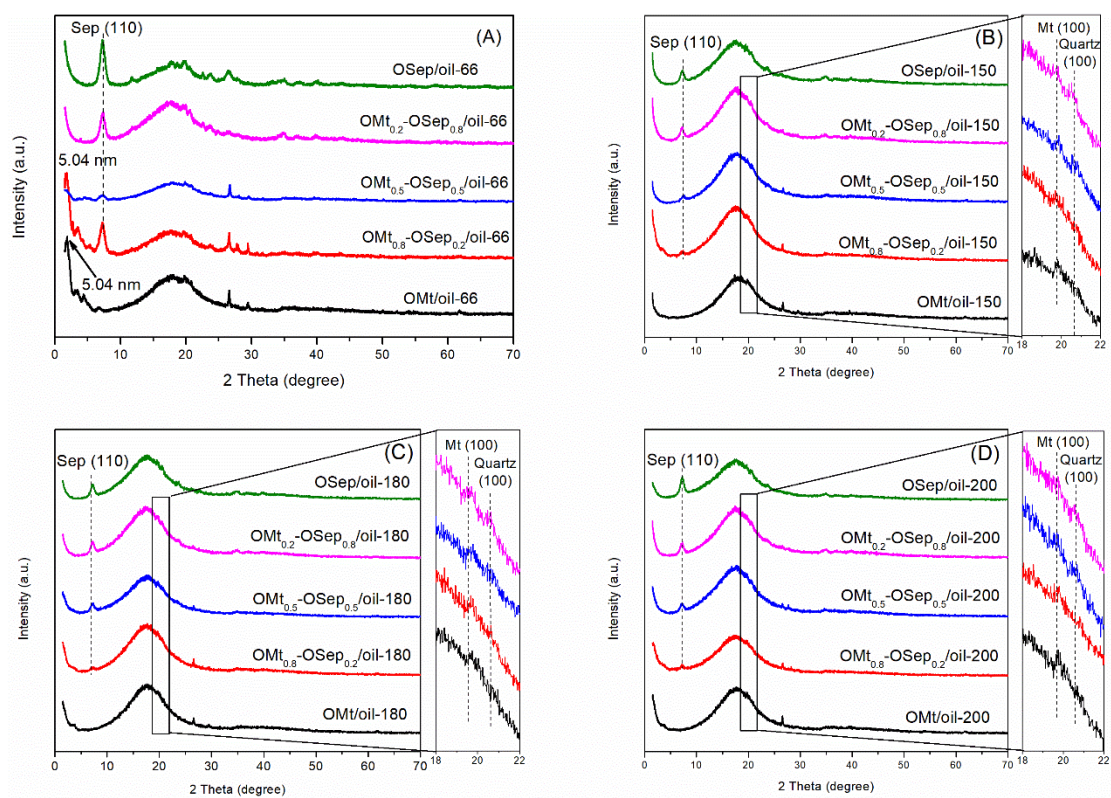of the sample holder and sample holder with oil.

Fig. 3 XRD patterns of OC/oil gels aged at (A) 66°C, (B) 150°C, (C) 180°C and 200°C.
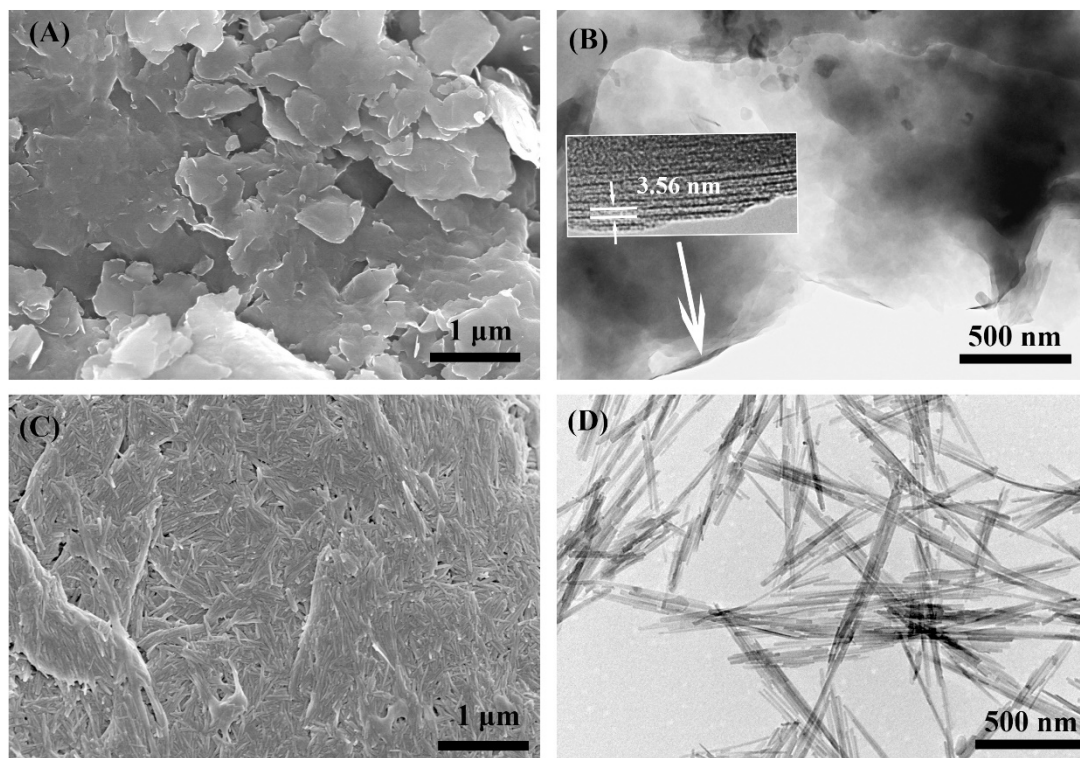

Fig. 4 SEM images of (A) OMt and (C) OSep; TEM images of (B) OMt and (D) OSep.
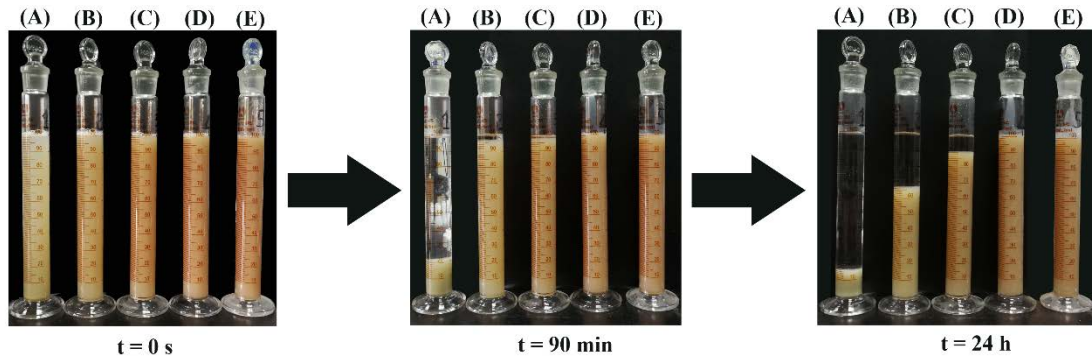
Fig. 5 Gel volume results of (A) OMt, (B) $OMt_{0.8}$-$OSep_{0.2}$, (C) $OMt_{0.5}$-$OSep_{0.5}$, (D) $OMt_{0.2}$-$OSep_{0.8}$ and (E) OSep in oil.

Fig. 6 Dynamic rheological curves of OC/oil fluids aged at (A) 66°C, (B) 150°C, (C) 180°C and (D) 200°C for 16 h.

Fig. 7 the Interpretive diagram of the network structure of the mixed OMt and OSep in oil.

Figure captions:

Fig. 1 XRD patterns of (A) Mt, OMt, (B) Sep and OSep.

Fig. 2 (A) Interpretive diagram of XRD test for OC/oil gel sample and (B) XRD patterns of the sample holder and sample holder with oil.

Fig. 3 XRD patterns of OC/oil gels aged at (A) 66°C, (B) 150°C, (C) 180°C and 200°C.

Fig. 4 SEM images of (A) OMt and (C) OSep; TEM images of (B) OMt and (D) OSep.

Fig. 5 Gel volume results of (A) OMt, (B) $OMt_{0.8}$-$OSep_{0.2}$, (C) $OMt_{0.5}$-$OSep_{0.5}$, (D) $OMt_{0.2}$-$OSep_{0.8}$ and (E) OSep in oil.
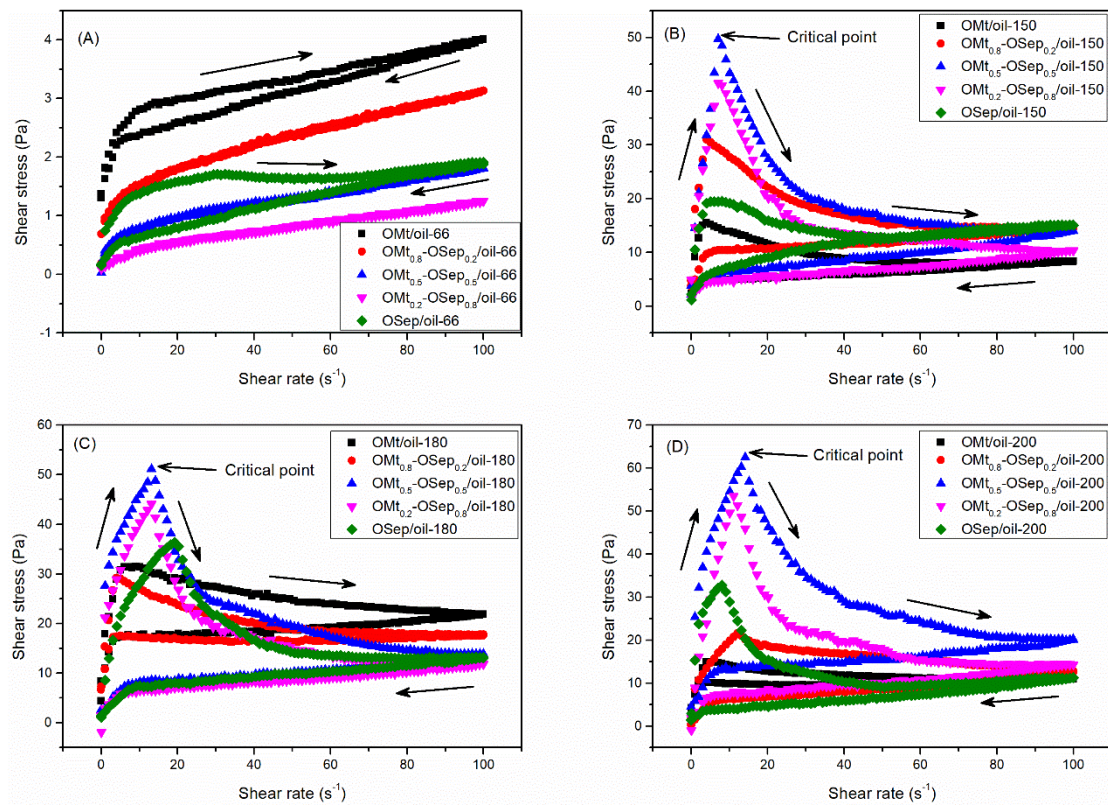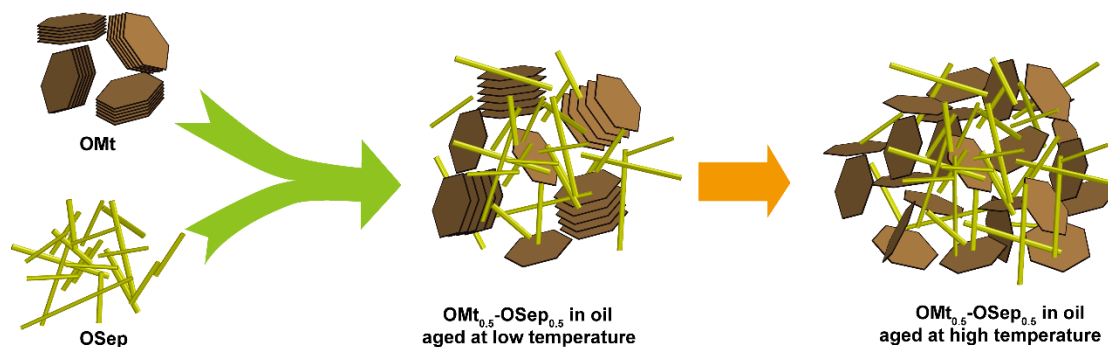
Fig. 6 Dynamic rheological curves of OC/oil fluids aged at (A) 66°C, (B) 150°C, (C) 180°C and (D) 200°C for 16 h.

Fig. 7 the Interpretive diagram of the network structure of the mixed OMt and OSep in oil.

Tables

Table 1 Chemical composition of Mt and Sep (derived from XRF results)

Sample	Composition (mass %)						
	SiO_2	Al_2O_3	CaO	MgO	Na_2O	Fe_2O_3	others
Mt	64.40	19.71	4.16	3.75	3.72	3.30	0.96
Sep	63.68	9.88	1.26	19.41	0.87	3.35	1.55

Table 2 Details of the mixtures of OMt and OSep.

Sample	OMt (mass %)	OSep (mass %)
OMt	100	0
$OMt_{0.8}$-$OSep_{0.2}$	80	20
$OMt_{0.5}$-$OSep_{0.5}$	50	50
$OMt_{0.2}$-$OSep_{0.8}$	20	80
OSep	0	100

Table 3 A summary of shear stress results corresponding to the critical points.

Sample	Shear stress (Pa)			
	66°C	150°C	180°C	200°C
OMt/oil	none	15.62	31.41	15.28
$OMt_{0.8}$-$OSep_{0.2}$/oil	none	31.50	29.33	22.05
$OMt_{0.5}$-$OSep_{0.5}$/oil	none	50.12	51.08	62.67
$OMt_{0.2}$-$OSep_{0.8}$/oil	none	41.52	44.49	53.81
OSep/oil	none	19.64	36.53	33.06

Table 4 A summary of shear stress (τ) at the shear rate (γ) of 100 s^{-1}.

Sample	τ (Pa)				τ_{66-150}	$\tau_{180-200}$
	66°C	150°C	180°C	200°C	(%)	(%)
OMt/oil	4.02	8.36	21.53	10.96	108	-49
$OMt_{0.8}$-$OSep_{0.2}$/oil	3.13	14.95	17.60	13.10	378	-26
$OMt_{0.5}$-$OSep_{0.5}$/oil	1.80	14.16	13.96	20.34	687	46
$OMt_{0.2}$-$OSep_{0.8}$/oil	1.25	9.95	11.78	13.86	696	18
OSep/oil	1.91	15.16	13.29	10.85	694	-18

Note: $\tau_{66-150} = (\tau_{150}-\tau_{66})/ \tau_{66} \times 100\%$, similarly, $\tau_{180-200} = (\tau_{200}-\tau_{180})/ \tau_{180} \times 100\%$; τ_x refers to the shear stress at 100 s^{-1} of fluids aged x°C.

Table 5 The areas of thixotropic loops (A) in Fig. 6.

Sample	A (Pa·s^{-1})				A_{66-150} (%)	$A_{180-200}$ (%)
	66°C	150°C	180°C	200°C		
OMt/oil	22.50	325.97	635.20	186.22	1349	-71
OMt$_{0.8}$-OSep$_{0.2}$/oil	3.46	600.86	710.46	361.12	17266	-49
OMt$_{0.5}$-OSep$_{0.5}$/oil	4.82	1097.75	1281.62	1497.10	22675	17
OMt$_{0.2}$-OSep$_{0.8}$/oil	2.39	907.37	1011.93	1080.78	37865	7
OSep/oil	39.38	275.34	842.99	644.85	599	-24

Note: $A_{66-150} = (A_{150}-A_{66})/A_{66} \times 100\%$, similarly, $A_{180-200} = (A_{200}-A_{180})/A_{180} \times 100\%$; A_x refers to the area of a sample aged at x°C.